

Anomalous x-ray diffraction study of disorders in epitaxial films of the Heusler alloy Co_2MnGe

Brian A. Collins

Department of Physics and Astronomy, University of North Carolina, Chapel Hill, North Carolina 27599-3255

Yuncheng Zhong and Yong S. Chu

Advanced Photon Source, Argonne National Laboratory, Argonne, Illinois 60439-4856

Liang He and Frank Tsui^{a)}

Department of Physics and Astronomy, University of North Carolina, Chapel Hill, North Carolina 27599-3255

(Received 6 November 2006; accepted 5 March 2007; published 31 May 2007)

The authors report a study of structural and chemical disorders in a ternary combinatorial epitaxial film of $\text{Co}_x\text{Mn}_y\text{Ge}_{1-x-y}$ in the composition range that includes the Heusler alloy Co_2MnGe , using microbeam anomalous x-ray diffraction techniques. The structural and chemical ordering of the alloy has been found to be extremely stable over a large composition range, while elemental site swapping and sublattice vacancies have been identified. A model of anomalous diffraction around the Co and Ge edges is presented and shown to make possible the identification and quantification of these disorders in an epitaxial film.

© 2007 American Vacuum Society. [DOI: 10.1116/1.2720857]

I. INTRODUCTION

As the size of electronic devices shrinks and as the demand for high speed information processing grows, research in spin-based electronics^{1,2} has also grown. One area of increasing interest has been that of half metals,² novel magnetic materials exhibiting 100% spin polarization at the Fermi level. These materials would be excellent candidates for electronic spin injectors and spin filters.² Some Heusler alloys, such as Co_2MnGe , have been predicted theoretically to be half metallic.³ However, experimentally the highest spin polarization reported to date for Heusler alloys is only 58%.⁴ The deficiency has been attributed to structural and chemical disorders, such as elemental site swapping,^{5,6} and to the off-stoichiometric nature of the samples studied.⁷

In this article we examine the various types of disorder in a ternary combinatorial epitaxial film of $\text{Co}_x\text{Mn}_y\text{Ge}_{1-x-y}$, using anomalous x-ray diffraction. The investigation has been focused in a compositional region that includes the Heusler alloy Co_2MnGe . The use of combinatorial molecular beam epitaxy (MBE) techniques makes it possible for systematic explorations of composition dependent phenomena in ternary systems. Our analyses rely on extensive and systematic modeling of anomalous x-ray diffraction intensities in order to enhance the sensitivity for studying different types of structural and chemical disorders. In the following section, we describe experimental techniques with emphasis on the anomalous x-ray diffraction technique and the crystal structure of the Heusler alloy. In Sec. III, we present results on detection and analyses of three types of disorders in the Heusler structure, namely, structural and chemical stacking (Sec. III A), elemental site swapping (Sec. III B), and site-specific

vacancies (Sec. III C). In a separate publication we present the detailed evolution of the disorders as a function of composition and the influence on magnetic properties.

II. EXPERIMENT AND CRYSTAL STRUCTURE

The ternary combinatorial sample of $\text{Co}_x\text{Mn}_y\text{Ge}_{1-x-y}$ was grown by combinatorial MBE on a Ge (111) substrate. A multilayer method, sequential deposition of monolayer wedges of each element, was employed for the combinatorial synthesis. Each monolayer wedge was deposited across the substrate by moving a precision shadow mask and was monitored by an element specific atomic absorption flux monitor, as detailed elsewhere.⁸ The film was grown at 250 °C at a deposition rate of 0.1 Å/s on top of a 200 Å Ge(111) buffer layer. Deposition was followed by a postgrowth annealing at 450 °C for 20 min. The thickness of the film was 630 ± 10 Å, as determined by x-ray diffraction (XRD) experiments using a crystal truncation rod analysis. Composition and structure were studied and quantified *ex situ* using microbeam x-ray fluorescence (XRF) spectroscopy and XRD techniques at XOR beamlines of the Advanced Photon Source (APS) Argonne National Laboratory.^{9,10} An earlier study shows that the epitaxial growth of this ternary system can be stabilized over nearly the entire composition range. Especially in the composition region near the Heusler alloy, the film exhibits a highly coherent structure with a face-centered-cubic (fcc) symmetry.¹¹

The anomalous x-ray diffraction technique involves diffraction as a function of incident photon energy through a characteristic absorption edge of an element. The work was carried out at the 2-BM beamline of the APS. The energy of the synchrotron x-ray source was selected using a water-cooled double-crystal Si(111) monochromator. Kirkpatrick-

^{a)}Electronic mail: ftsui@physics.unc.edu

TABLE I. Three unique Bragg reflections of the Heusler structure are shown in both the traditional cubic notation and the convenient hexagonal notation (Ref. 10). The stars indicate that the reflection studied was the 60°-rotated twin about the [111] direction. Also shown are the structure factors corresponding to each reflection and the selection rules for the three families of reflections.

Studied reflection		Structure factor	Bragg condition
Cubic	Hexagonal		
(022)*	(104)*=(014)	$3f_{\text{Ge}}+3f_{\text{Mn}}+6f_{\text{Co}}$	If $H+K+L=2\times\text{even}$
(002)*	(012)*=(102)	$3f_{\text{Ge}}+3f_{\text{Mn}}-6f_{\text{Co}}$	If $H+K+L=2\times\text{odd}$
(111)*	(101)*=(011)	$3f_{\text{Ge}}-3f_{\text{Mn}}$	If $H+K+L=\text{odd}$

Baez x-ray mirrors were used to focus the beam to a spot size of 2–10 μm in both the horizontal and vertical directions, resulting in a maximum composition spread within the beam of about 0.1%. A Huber four-circle diffractometer equipped with a precision xyz stage was used for the diffraction study to probe different locations on the combinatorial sample, while a Si-drift diode energy dispersive fluorescence detector was used to simultaneously monitor the composition.

The energy of the incident beam was calibrated by fluorescence x-ray-absorption fine structure using Co and Ge NIST standards. In order to ensure the same beam position on the sample (the same composition) regardless of which energy range was used and which reflections were measured, the beam position and shape were checked at each of the three elements' excitation energies, and detailed fluorescence maps of the sample were made for each of the Bragg reflections studied. To obtain the intensity as a function of energy at a particular sample position (composition), the Bragg reflection was first located in reciprocal space via in-plane and out-of-plane scans. Following this, the diffractometer was set to the observed peak position of the reflection, and the energy was scanned while the diffractometer was continuously adjusted to maintain a constant magnitude of momentum transfer (q). These scans were taken in a region of the sample that contains the Heusler stoichiometry.

Full Heusler alloys crystallize in the $L2_1$ structure, which consists of four interpenetrating fcc sublattices. For the Co_2MnGe , Ge atoms are located at the so-called $4a$ sites, Mn on the corresponding $4b$ sites, and Co on the $8c$ sites that occupy two of the fcc sublattices. Reference 3 provides an excellent visualization for the structure in both the (001) and (111) orientations. The $L2_1$ crystal structure produces three unique families of Bragg reflections: one “fundamental” {022} and two “superstructure” {002} and {111} reflections.¹² These reflections and their attributes are listed in Table I. The fundamental reflection is insensitive to chemical disorder, being the simple sum of the atomic form factors, whereas the superstructure reflections involve differences of sublattice form factors.¹³ The differences within the structure factors make the resulting diffraction intensities both above and below the x-ray absorption edges sensitive to chemical disorders.

The three unique Bragg reflections were modeled for various types of disorder and compared with the measurements obtained at different compositions. The energy E and momentum dependent diffraction intensity has been modeled using

$$I(\mathbf{q}, E) = \alpha \left| \sum_n [f_n^0(\mathbf{q}) + f_n'(E) + i f_n''(E)] e^{i\mathbf{q}\cdot\mathbf{r}_n} \right|^2 A(\mathbf{q}, E). \quad (1)$$

Here, the atomic form factor at the atomic position \mathbf{r}_n is expressed within the square bracket in terms of the energy-independent component f^0 , and the real (f') and imaginary (f'') anomalous corrections, and is summed over all the atoms within the unit cell. The values of these were tabulated originally by Cromer and Liberman¹⁴ and ported subsequently to an IGOR library.¹⁵ The self-absorption attenuation $A(\mathbf{q}, E)$ was modeled based on the sample and diffraction geometries using the linear absorption coefficients from the library mentioned above. This factor, however, was found to have a negligible effect on the diffraction intensities since the film was only 630 Å thick. The overall scaling factor α was used to scale the fits with the data. A weighted elemental scattering factor has been used to model the disorder at each atomic position within the unit cell as given by

$$I(\mathbf{q}, E) = \alpha \left| \sum_n [x_n f_{\text{Co}}(\mathbf{q}, E) + y_n f_{\text{Mn}}(\mathbf{q}, E) + z_n f_{\text{Ge}}(\mathbf{q}, E)] e^{i\mathbf{q}\cdot\mathbf{r}_n} \right|^2 A(\mathbf{q}, E), \quad (2)$$

where the atomic form factor $f(\mathbf{q}, E)$ for each element with its anomalous corrections [Eq. (1)] is scaled by the corresponding occupation coefficient (x , y , and z). The current model, however, does not include solid-state effects¹⁶ that give rise to fine structures above the absorption edge. A more complete model that accounts for these effects will be reported elsewhere.

III. RESULTS AND DISCUSSION

A. Structural and chemical stacking sequence

For a (111) film, a particular stacking and chemical sequence must be observed for the Heusler structure since the (111) orientation is prone to stacking faults in cubic systems. To that end hundreds of possible sequences have been modeled and compared with the diffraction data. Figure 1 illustrates three examples of the models for the anomalous diffraction intensities near the Co edge with unit cells containing correct chemical ordering but with different structural stacking sequences. The behavior for the Heusler structure with fcc stacking is shown in Figs. 1(a)–1(c) for all three Bragg reflections. The features in the model can be easily understood by referencing the corresponding structure factor in Table I. Figures 1(d)–1(i) show two other possible stacking sequences, each exhibiting qualitative features easily distinguishable from those of the correct Heusler stacking sequence. Among all the sequences modeled, the Heusler structure exhibits a unique set of features in the anomalous diffraction intensities.

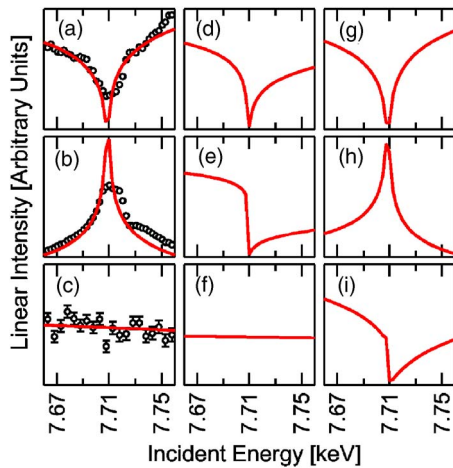


FIG. 1. Examples of models for different stacking sequences of the unit cell. Each plot is linear intensity vs energy near the Co edge (7.66–7.76 keV). The rows of plots show behaviors for various reflections: the top row, (022); the middle row, (002); and the bottom row, (111). Columns of plots show the corresponding behaviors for various stacking sequences: [(a)–(c)] the Heusler stacking (ABC ABC ABC ABC), [(d)–(f)] (ABC ACB ABC ACB), and [(g)–(i)] (ACB ACB ABC ABC). Lines correspond to models, and circles in (a)–(c) are data taken near the Heusler stoichiometry.

A set of scans taken near the Heusler stoichiometry on our ternary sample is shown with the model in Figs. 1(a)–1(c). They exhibit a remarkable resemblance to the Heusler structure and thus can be distinguished from all other models studied. As noted above, the solid-state effects giving rise to the fine structures in the data above the absorption edge are not modeled in this study, but they would not affect the qualitative features in the models presented here.

Figure 2 shows several models with different chemical stacking sequences in the same energy range as those shown in Fig. 1. Again, Figs. 2(a)–2(c) show the behaviors of three

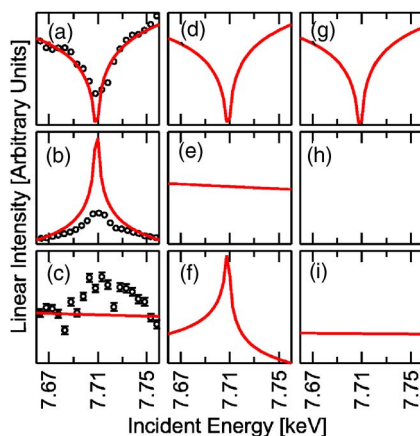


FIG. 2. Examples of models for different chemical sequences of the unit cell. The axes of each plot and the arrangement of rows of panels are the same as in Fig. 1. Columns of plots show the behaviors for various chemical stacking sequences: [(a)–(c)] Heusler stacking with chemical sequence three times of GeCoMnCo, [(d)–(f)] three times of GeMnCoCo, and [(g)–(i)] twice of GeCoGeMnCoGe. The absence of a plot in (h) is a result of the forbidden Bragg reflection for the chemical sequence. The same as in Fig. 1. Lines correspond to models, and circles in [(a)–(c)] are data taken near the composition of Co_2MnGe_3 , thus off the Heusler stoichiometry.

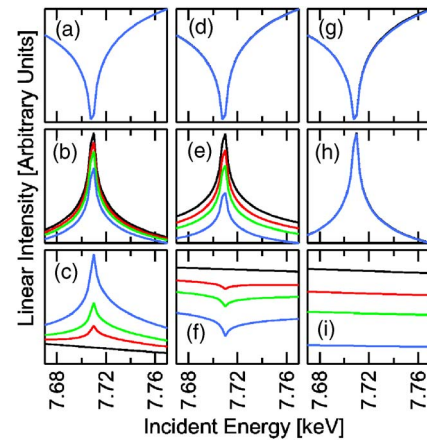


FIG. 3. Progression of antite disorders (site swapping) in the Heusler structure. The axes of each panel and the arrangement of the rows are the same as the ones in Fig. 1. The columns correspond to models of three different antite disorders: [(a)–(c)] Co–Mn site swapping, [(d)–(f)] Co–Ge site swapping, and [(g)–(i)] Ge–Mn site swapping. Within each panel there are four lines that correspond to the various amounts of site swapping: 0%, 5%, 10%, and 20% with respective colors of black, red, green, and blue. In each case the (022) or the fundamental Bragg reflection is unchanged, providing the basis for making quantitative comparisons in the other two reflections.

unique Bragg reflections for the Heusler structure with sequence three times of Ge–Co–Mn–Co. In contrast, Figs. 2(d)–2(f) show the behavior of a unit cell containing the same stoichiometry but with an alternative sequence of three times Ge–Mn–Co–Co. A different stoichiometry is modeled in Figs. 2(g)–2(i), illustrating what the behavior might look like at the composition near Co_2MnGe_3 . Here, the data from composition approximately Co_2MnGe_3 are shown with the model in Figs. 2(a)–2(c). Although the fits are not nearly as good as those shown in Fig. 1, the data can still be distinguished from the other models. In all, approximately 100 models were explored by changing the chemical sequence as well as the stacking sequence, layer number, and even the layer configuration (e.g., that for the diamond lattice). All of these suggest that anomalous diffraction can be used to distinguish the Heusler structure from others. The fact that the Heusler chemical and structural ordering is seen in compositions far from the correct stoichiometry reinforces the established notion that this structure is very stable.

B. Elemental site swapping

Although stacking and chemical sequences could become a variable in this growth direction, by far the most predicted source of disorder in the Heusler structure has been elemental site swapping. Neutron diffraction experiments⁶ have shown to be helpful in uncovering several types of disorders in bulk samples; however, thin film samples lack the volume necessary for a neutron experiment. Recently, Ravel *et al.*⁷ have shown that synchrotron-based anomalous diffraction could be used to probe one type of disorder by studying the (111) reflection. Models of anomalous diffraction near the Co edge of all three reflections, as shown in Fig. 3, indicate that each of the three possible types of elemental site swapping can be probed individually using this method.

Figures 3(a)–3(c) show the progression of anomalous diffraction with increasing amounts of Co–Mn site swapping for each of the unique Bragg reflections. The counterparts for Co–Ge and Mn–Ge site swapping are shown in Figs. 3(d)–3(f) and Figs. 3(g)–3(i), respectively. The (022) reflection, as shown in the top row of Fig. 3, exhibits no sensitivity to the chemical disorder. This is consistent with the fact that the structure of the fundamental reflection is the sum of all the atomic form factors (Table I).

With increasing amounts of Co–Mn and Co–Ge site swapping, the superstructure peak (002) intensities decrease, as shown in Figs. 3(b) and 3(e), respectively. The ratio of intensities at the Co edge to the intensities away from the edge also decreases, as the level of disorder increases. In contrast, as shown in Fig. 3(h), the (002) reflection is not affected by the Ge–Mn site swapping because the sites nominally occupied by Ge and Mn are combined as a simple sum in this reflection, similar to the fundamental (Table I).

The models for the (111) reflection are shown in the bottom row of Fig. 3. Since the sublattice nominally occupied by Co does not contribute to this reflection, no feature exists at the Co edge for the perfect Heusler structure. In Fig. 3(c) the effects of Co–Mn swapping appear as a peak in the anomalous diffraction, owing to Co diffraction in this site. As the energy approaches the Co edge, its scattering factor is reduced due to increased absorption, causing a dip in scattering at that energy. Since Co and Mn have similar scattering factors, both smaller than Ge, the difference in the structure factor is accentuated at the Co edge, giving rise to the peak in the intensity.

The opposite effect can be seen in Fig. 3(f), where Ge swaps with Co. Because the larger scatterer (Ge) is replaced by one containing a characteristic dip, a dip emerges in the anomalous diffraction. Furthermore, owing to the different overall magnitudes in their structure factor, the intensity away from the Co edge also decreases. Finally, no effect in anomalous diffraction occurs for Ge–Mn swapping at this reflection [Fig. 3(i)] since neither of these elements have features at the Co edge, but the overall intensity falls rapidly with increasing swapping as the two terms in the structure factor become equal (Table I).

When multiple types of disorder occur, anomalous diffraction from just one reflection can be difficult to interpret. For example, the (111) reflection shows two opposing trends depending on the type of disorder present. If both occur equally, then the two effects could cancel, and no feature would be seen in the data. However, by comparing all three reflections' intensities and energy features, a unique solution for the quantification of the three types of site swapping can be obtained. This is where the fundamental reflection's insensitivity to chemical disorder is useful, as it becomes the basis with which to compare the other reflections' intensities. Studying the (111) reflection, a peak or trough in the anomalous diffraction can determine the amounts of Co–Mn swapping *relative* to those of Co–Ge. The combined amount of these two types of disorder can be determined by monitoring the size of the (002) reflection's energy peak. Thus, these two

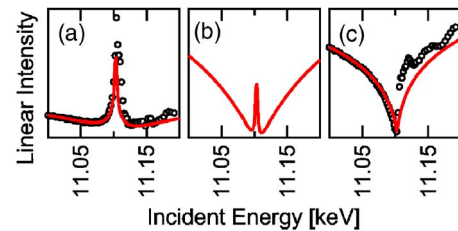


FIG. 4. Models (lines) and measured intensities (circles) for the (002) reflection near the Ge edge (11.0–11.2 keV) at various amounts of vacancies in the Co sublattice: (a) measured intensity near the Heusler stoichiometry and a model with 5% vacancy, (b) a model with 10% vacancy, and (c) measured intensity near 50 at. % Ge (Co_2MnGe_3) and a model with 18% vacancy.

types of disorder can be distinguished and quantified. The third type of disorder can be determined by simultaneously comparing the relative intensities of the (111) reflection to the (002) and the relative intensities of the (002) to the fundamental reflection. These effects were seen in the anomalous diffraction study of our ternary sample in the region surrounding the Heusler composition. The full analysis of site swapping with respect to composition will be reported elsewhere.

C. Vacancies

A final type of disorders, vacancies in the Co sublattice, has been modeled, and the results for the (002) reflection near the Ge edge with various levels of vacancies are shown in Fig. 4. The behavior exhibits dramatic changes in energy dependence with increasing vacancies from that of a peak at full occupancy to a characteristic dip at levels of $\sim 20\%$ vacancy. Data from both near the Heusler stoichiometry [Fig. 4(a)] and from that of Co_2MnGe_3 [Fig. 4(c)] are shown with the models demonstrating the presence of this type of disorder in our sample. The intensity and curvature of the anomalous data below the Ge edge are sensitive only to this type of disorder, as others show negligible effects.

IV. SUMMARY

We have grown a ternary combinatorial epitaxial film of $\text{Co}_x\text{Mn}_y\text{Ge}_{1-x-y}$ that contains the Heusler alloy Co_2MnGe . At and around this composition, we have developed and conducted experiments based on the technique of anomalous diffraction that is sensitive to many diverse forms of disorders. Our investigation shows that the structural and chemical stacking sequences of the Heusler structure are very stable, and that these experiments can be used to obtain quantitative values of the amounts of various disorders, including Co–Mn, Co–Ge, and Mn–Ge site swapping, and Co sublattice vacancies.

ACKNOWLEDGMENTS

The authors thank S. Vogt for the use of the XRF analysis software and J. Ilavsky for the use of the IGOR code, calculating atomic scattering and absorption factors. The work is supported in part by NSF No. DMR-0441218 for MBE synthesis, by DOD No. W911NF-05-1-0173 for MBE instru-

mentation, and by DOE No. BES DE-FG02-05ER46216 for the measurements and student support for two of the authors (B.A.C. and L.H.). An APS Subcontract No. 5F-00428 for partial student support for another author (B.A.C.) is also gratefully acknowledged. Use of the Advanced Photon Source is supported by the U.S. Department of Energy, Office of Sciences, Office of Basic Energy Sciences, under Contract No. DE-AC02-06CH11357.

¹G. A. Prinz, *Phys. Today* **48**(4), 58 (1995); G. A. Prinz, *Science* **282**, 1660 (1998).

²S. A. Wolf, D. D. Awschalom, R. A. Buhrman, J. M. Daughton, S. von Molnar, M. L. Roukes, A. Y. Chtchelkanova, and D. M. Treger, *Science* **294**, 1488 (2001).

³S. Ishida, T. Masaki, S. Fujii, and S. Asano, *Physica B* **245**, 1 (1998); S. Ishida, S. Fujii, H. Nagayoshi, and S. Asano, *ibid.* **254**, 157 (1998).

⁴R. J. Soulen, Jr. *et al.*, *Science* **282**, 85 (1998).

⁵D. Orgassa, H. Fujiwara, T. C. Schulthess, and W. H. Butler, *Phys. Rev. B*

60, 13237 (1999); S. Picozzi, A. Continenza, and A. J. Freeman, *Phys. Rev. B* **69**, 094423 (2004).

⁶B. Ravel, M. P. Raphael, V. G. Harris, and Q. Huang, *Phys. Rev. B* **65**, 184431 (2002).

⁷B. Ravel, J. O. Cross, M. P. Raphael, V. G. Harris, R. Ramesh, and V. Saraf, *Appl. Phys. Lett.* **81**, 2812 (2002).

⁸F. Tsui and L. He, *Rev. Sci. Instrum.* **76**, 062206 (2005).

⁹S. Vogt, Y. S. Chu, A. Tkachuk, P. Ilinski, D. A. Walko, and F. Tsui, *Appl. Surf. Sci.* **223**, 214 (2004).

¹⁰Y. S. Chu *et al.*, *Appl. Surf. Sci.* **223**, 175 (2004).

¹¹F. Tsui, L. He, D. Lorang, A. Fuller, Y. S. Chu, A. Tkachuk, and S. Vogt, *Appl. Surf. Sci.* **252**, 2512 (2006).

¹²P. J. Webster, *J. Phys. Chem. Solids* **32**, 1221 (1971).

¹³B. E. Warren, *X-Ray Diffraction* (Dover, New York, 1990), pp. 208–216.

¹⁴D. T. Cromer and D. Liberman, *J. Chem. Phys.* **53**, 1891 (1970).

¹⁵J. Ilavsky, Atomic scattering factors and attenuation using the Cromer-Liberman code for IGOR PRO ver. 4.0, 2006 (<http://www.uni.aps.anl.gov/~ilavsky/AtomicFormFactors.html>).

¹⁶J. O. Cross *et al.*, *Phys. Rev. B* **58**, 11215 (1998).